Article

# RNA Pore Translocation with Static and Periodic Forces: Effect of Secondary and Tertiary Elements on Process Activation and Duration

*Published as part of The Journal of Physical Chemistry virtual special issue "Ruth Nussinov Festschrift".*

Matteo Becchi,[#] Pietro Chiarantoni,[#] Antonio Suma, and Cristian Micheletti*

Cite This: *J. Phys. Chem. B* 2021, 125, 1098–1106

Read Online

ACCESS | Metrics & More | Article Recommendations

**ABSTRACT:** We use MD simulations to study the pore translocation properties of a pseudoknotted viral RNA. We consider the 71-nucleotide-long xrRNA from the Zika virus and establish how it responds when driven through a narrow pore by static or periodic forces applied to either of the two termini. Unlike the case of fluctuating homopolymers, the onset of translocation is significantly delayed with respect to the application of static driving forces. Because of the peculiar xrRNA architecture, activation times can differ by orders of magnitude at the two ends. Instead, translocation duration is much smaller than activation times and occurs on time scales comparable at the two ends. Periodic forces amplify significantly the differences at the two ends, for both activation times and translocation duration. Finally, we use a waiting-times analysis to examine the systematic slowing downs in xrRNA translocations and associate them to the hindrance of specific secondary and tertiary elements of xrRNA. The findings provide a useful reference to interpret and design future theoretical and experimental studies of RNA translocation.
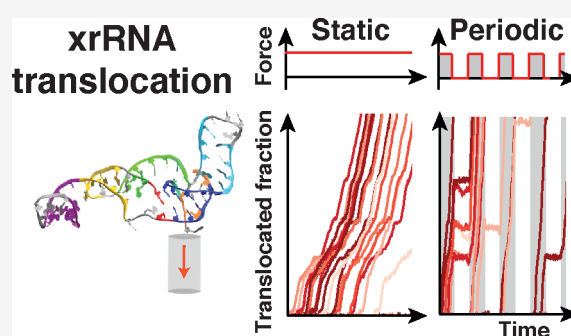
## INTRODUCTION

RNA translocation is a rapidly growing avenue in theoretical and experimental single-molecule studies. Pore translation has recently allowed for distinguishing different types of tRNAs[1] and quantifying mRNA expression.[2] Measurements of ionic current blockades in nanopores[3] have been used to sequence RNAs[4] to probe salient features of their folding pathway[5] and to detect modified nucleobases.[6] Molecular dynamics simulations have shown that driving RNAs through pores of appropriate width can relay information about their compliance to structural deformations[7] and directional mechanical resistance.[8]

RNA translocation properties are of direct biological relevance, too, as they determine the interaction with and response to processive enzymes. For instance, sequences and structures of viral RNAs have evolved to introduce specific ribosomal slippages needed to produce alternative transcripts.[9−12] Arguably, the most striking example of viral RNA hindrance to enzymatic translocation is given by xrRNAs. These molecules are about 70 nucleotides long, rich in pseudoknots, and can resist degradation by exonucleases while remaining processable by other enzymes.[13−18]

In a recent theoretical and computational study from our group,[8] atomistic simulations of Zika xrRNA translocation

were used to explore the microscopic origin of its resistance to degradation. The xrRNA structure (see Figure 1) is organized so to produce very different structural deformations when one or the other termini are engaged and translocated through the pore. These directional dependent deformations allow the xrRNA to withstand translocation very differently at the two ends. By far, the largest hindrance is encountered at the 5′ terminal, which is the same one attacked by exonucleases.[15] Such major directional response is arguably what makes xrRNA resistant to degradation (initiating at the 5′ end) while still processable for transcription and replication (initiating at the 3′ end).
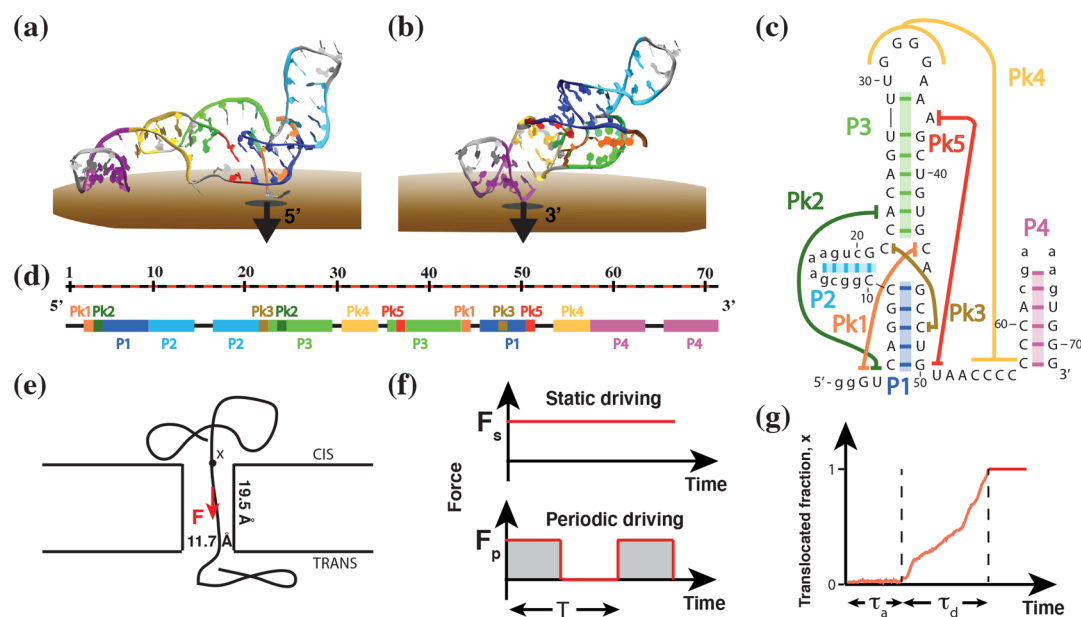
For both its biological relevance and atypical density of pseudoknots, xrRNA is an ideal substrate to study how the translocation process depends on intrinsic properties, such as secondary and tertiary elements, and extrinsic ones, such as the use of static or periodic pulling modes.
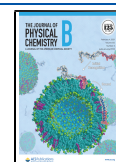
**Figure 1.** System setup. Typical configurations at the beginning of translocation simulations from the (a) 5′ and (b) 3′ ends of Zika xrRNA. The molecule is organized in four helices (P1−P4) and five pseudoknots (Pk1-Pk5), as represented in panels c and d by using the same color code of panel a. Specifically, in the two-dimensional graph of panel c, the backbone connectivity is subsumed by the sequential numbering of the nucleotides, which are indicated with their one-letter code, and the colored dashes and lines indicate the main pairings and interactions of helices and pseudoknots. In panel d, the same motifs are annotated along the one-dimensional representation of the xrRNA. During translocation, the molecule is driven through a cylindrical pore (e) by means of a static or periodic force (f) that is distributed and applied on the P atoms that are inside the pore. (g) The translocation progress is monitored via the fraction of translocated atoms, $x$, whose time evolution is sketched in panel g along with the indication of the activation time, $\tau_a$, and duration, $\tau_d$, of the translocation process. Zika xrRNA's structure was rendered with the VMD graphical package.[22] The scheme in panel c is adapted with permission from ref 8.

Studying the role of secondary and tertiary elements is important from the polymer physics point of view, as it aptly complements the now well-established theory of translocating homopolymers.[19−21] The latter enjoy a large conformational freedom, and their out-of-equilibrium translocation response can significantly depend on how tension propagates along the fluctuating backbone. By contrast, folded RNAs are structurally constrained by intramolecular interactions, including base pairings, that introduce translocation barriers that have no counterpart in homopolymers.

The effect of using different driving modes is of interest, too, for at least two reasons. First, to our knowledge, it has not been considered before in connection with RNAs. Second, periodic driving offers a simplified model of translocation as operated by processive enzymes, which pull on the substrate intermittently.

Here we will address these largely unexplored avenues using molecular dynamics simulations on a native-centric atomistic model of Zika xrRNA. In our study, which adopts the same setup of ref 8, we study how the xrRNA responds when driven from either of its ends through a narrow pore by static and periodic forces. In particular, we examine the translocation duration and activation times and discuss how they significantly vary with the magnitude and period of the driving force and with pulling directionality, that is, whether one or the other xrRNA ends are initially engaged. Finally, we examine the so-called waiting times profiles to rationalize the systematic nonuniformities of the translocation process and relate them to the hindrance offered by xrRNA's secondary and tertiary motifs.

## METHODS

**xrRNA Structure.** We considered the 71-nucleotide-long Zika xrRNA structure of PDB[23] entry 5TPY,[15] which is shown in Figure 1. The molecule features five relatively short pseudoknots, labeled Pk1 to Pk5, mostly concentrated at the 5′ end, and four helices, P1 to P4 (see Figure 1). Two- and one-dimensional representations of the secondary and tertiary motifs are given in Figure 1c,d.

**System Setup.** Following ref 8, the 5′ and the 3′ xrRNA ends were separately primed at the entrance of a narrow cylindrical pore embedded in a parallelepiped slab (see Figure 1a,b,e). The pore is 11.7 Å wide and 19.5 Å long, approximating the lumen of the Xrn1 exoribonucleases.[24]

To treat xrRNA intramolecular interactions, we used SMOG,[25,26] an implicit-solvent atomistic force field that is native centric. As such, the potential energy, which includes bonded and nonbonded interactions, angular and dihedral terms, is designed to stabilize the native conformation. Excluded volume interactions of the xrRNA with the pore and slab walls were accounted for with truncated and shifted Lennard-Jones potentials.

Constant temperature (Langevin) translocation simulations were performed with the LAMMPS package[27] after conversion of the input and topology files by using the "SMOG-converter" that is publicly available on the github repository.[28] Following ref 8, the system temperature and energy scale were calibrated by matching the typical stretching forces (∼15 pN) required to unfold small RNA helices at 300 K. Simulations were performed with proper atomic masses and with default values of the friction coefficient.

The characteristic simulation time is $\tau_{MD} = \sigma\sqrt{m/\epsilon}$, where the typical range and strength of interaction potentials are $\sigma =$
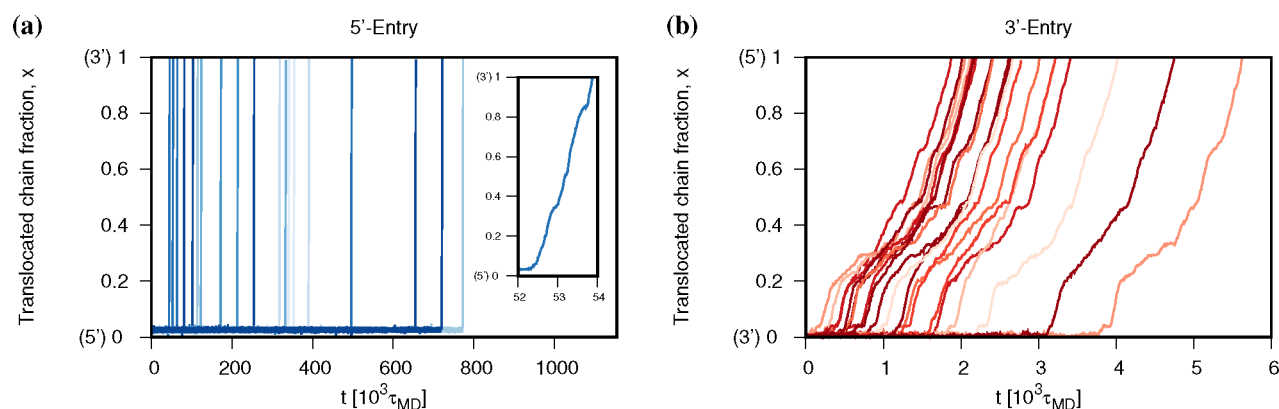
**Figure 2.** Translocation curves at constant driving force. Translocation curves at $F_s$ = 210 pN for 5′ (blue) and 3′ (red) entries of Zika xrRNA. Twenty independent trajectories are shown in both cases. Because the activation time at the 5′ end is much longer than the duration of translocation, the postactivation $x(t)$ curves are too steep to show discernible features. The latter can be appreciated in the inset, which shows the postactivation $x(t)$ curve for a single run.
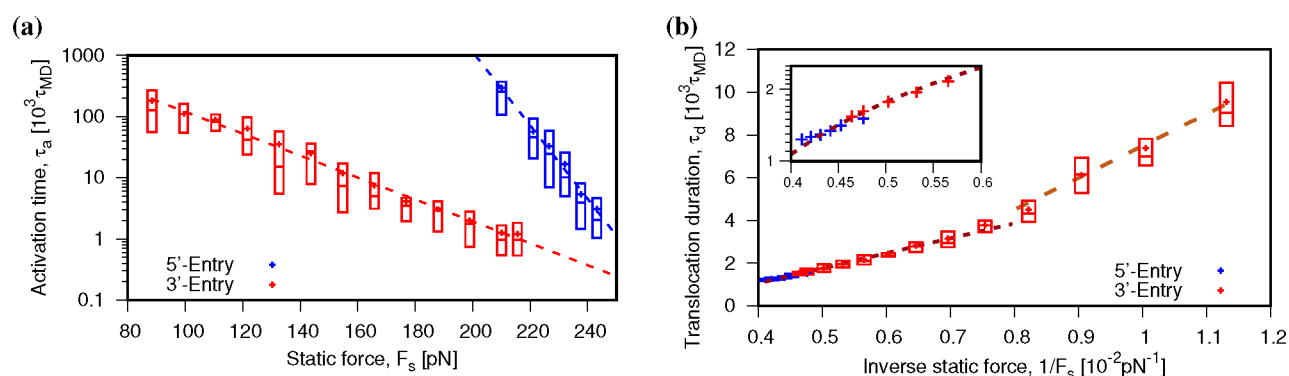


**Figure 3.** Translocation activation times and process duration at constant driving forces. Box plots for (a) translocation activation times, $\tau_a$, and (b) translocation duration, $\tau_d$, for 5′ (blue) and 3′ (red) entries for various static driving forces, $F_s$ (dot, average; center line, median; box limit, upper and lower quartile). The dashed lines in (a) are exponential best fits for $\tau_a$ and correspond to barrier widths of $\Delta_{5'}$ = 5.6 ± 0.2 Å and $\Delta_{3'}$ = 1.69 ± 0.04 Å. Panel b illustrates the dependence of $\tau_d$ on the inverse force. Two main regimes are apparent for the 3′ case. Their linear best fits (dashed lines) yield a crossover at $F_s^{-1} \sim 0.76 \times 10^{-2}$ pN$^{-1}$. The response at small $F_s^{-1}$ values, i.e., large forces, is highlighted in the inset, where the distinct trends of the 5′ and 3′ entries are better appreciated.

4 Å and $\epsilon$ = 0.1 kcal/mol, respectively, and $m$ = 15 amu.[8] The integration time step was set equal to $8.7 \times 10^{-4}$ $\tau_{MD}$. The nominal mapping of simulation units to real units yields $\tau_{MD} \sim$ 1.3 ps, though the absence of explicit solvent interactions is expected to skew the model dynamics to being faster than it actually is by orders of magnitude.[29] For this reason, temporal durations are expressed in units of $\tau_{MD}$ throughout the study.

After a preliminary relaxation run, the molecule was translocated by an external force. We considered two different driving protocols: one with a static force, $F_s$, and one with a periodic force switched regularly between 0 and $F_p$ (square wave). To mimic electrokinetic translocations, the driving force was applied only to the $P$ atoms inside the pore. Because the latter can fluctuate in number, the total force, $F_s$ or $F_p$, was equally subdivided among the $P$ atoms in the pore. For each considered value of the force and switching rate, we collected from 20 to 40 independent runs.

**Observables.** The progress of the translocation process was monitored via the translocated chain fraction, $x$, defined as the fraction of xrRNA atoms that have left the *cis* region, and thus are either in the pore or in the *trans* region.

The translocation activation time, $\tau_a = t_{start} - t_0$, measures the time elapsed from the start of the simulation, $t_0$, to when the leading P atom reaches the *trans* region without retracting

from it, $t_{start}$. This condition corresponded to the onset of irreversible translocations for all combinations of static and periodic drivings. The translocation duration, $\tau_d = t_{end} - t_{start}$, measures the time elapsed from the process activation, $t_{start}$, to when the last xrRNA atom enters the *trans* region, $t_{end}$.

To characterize the translocation hindrance of different xrRNA regions, we measured the so-called waiting time[30] for each nucleotide. This observable, $w$, is the cumulative time that a nucleotide spends straddling the pore entrance, i.e., with part of its atoms in the *cis* region and others inside the pore. Such "straddling time" may be cumulated over multiple time intervals (in the case of retractions) and is averaged over different simulations.

## ■ RESULTS AND DISCUSSION

Recent work from our group has demonstrated a strong directional response of Zika xrRNA to translocation, with the 5′ end offering much more resistance than the 3′ one. The enhanced resistance originates from the peculiar geometry of the pseudoknotted 5′ end, which is encircled by secondary elements that tighten up when the driving force pulls them against the pore rim.[8] These results were established by using a force-ramping protocol, a common setup in force-spectroscopy experiments.
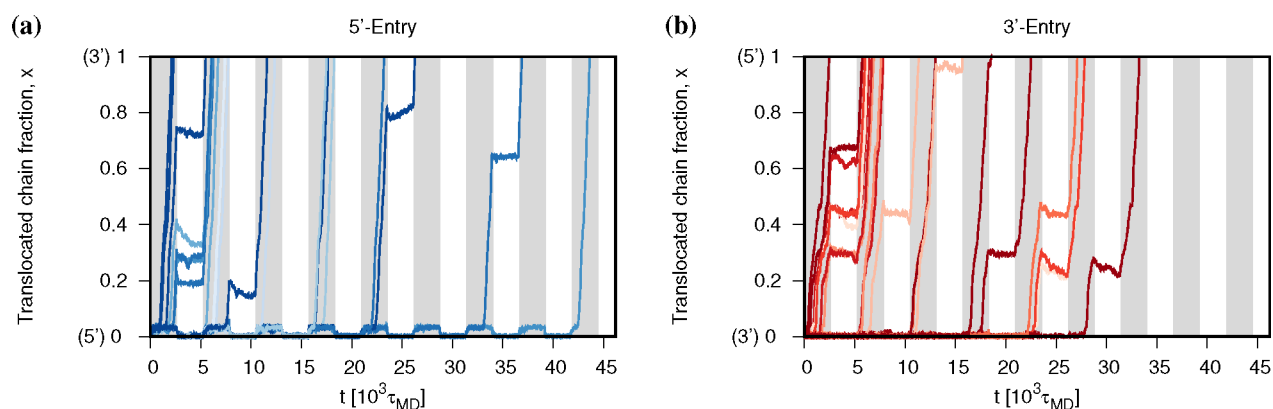
**Figure 4.** Translocation curves for a periodic driving force. Translocation curves for 5′ (blue) and 3′ (red) entries driven by a periodically switched force, $F_p$. The latter was set equal to 238 and 177 pN at the 5′ and 3′ ends, respectively, so to have comparable activation times (see Figure 3a). A shaded background highlights the semiperiods when the driving is "on". In the "off" semiperiods, one notices pauses and even chain retractions from the pore.

Here, we consider different pulling protocols: first, a static mode with a constant driving force, $F_s$, and then a periodic mode, where the driving force is switched between 0 and $F_p$ at regular intervals of duration $T/2$ (see Figure 1f).

**Static Driving.** *Activation Time.* For general homopolymers, translocation initiates as soon as the driving force is applied, provided that the latter overcomes the chain's entropic recoil. This is not the case for the considered system, where intramolecular interactions, such as base pairings, allow the molecule to withstand the exerted force and delay the onset, or activation, of translocation.

This is illustrated by the typical translocation curves of Figure 2, portraying the time evolution of the translocated chain fraction, $x$, for a constant force $F_s = 210$ pN.

The $x$-axis scales of the two graphs reveals a striking difference of activation times, $\tau_a$, at the two xrRNA ends: the average $\tau_a$ is $1.25 \times 10^3 \, \tau_{MD}$ for the 3′ entry and $294 \times 10^3 \, \tau_{MD}$ for the 5′ end, a 2 order of magnitude difference. Note that the translocation process at the 3′ end not only initiates but also completes in a time span much smaller than the activation time at the 5′ end. This implies that the entire molecule, including the portion resisting translocation at the 5′ end, is disrupted significantly faster from the 3′ end.

A systematic comparison of the activation times, $\tau_a$, for 5′ and 3′ pore entries is given in Figure 3. The linear trends in the semilog plot of Figure 3a indicate that $\tau_a$ decays about exponentially with the applied force at both ends, $\tau_a \propto e^{-\beta F_s \Delta}$. Thus, notwithstanding the complex interactions of the xrRNA termini and the pore, the activation of translocation can be modeled as a two-state process involving a free energy barrier of effective width $\Delta$.

The exponential best fits of the $\tau_a$ data, shown by the dashed lines in Figure 3a, yield $\Delta_{5'} = 5.6 \pm 0.2$ Å for the 5′ entry and $\Delta_{3'} = 1.69 \pm 0.04$ Å for the 3′ one. The values of the effective barrier widths are similar to those established from the Bell–Evans analysis of force-ramped translocations,[8] $\Delta_{5'}^{BE} = 4.4 \pm 0.4$ Å and $\Delta_{3'}^{BE} = 2.0 \pm 0.1$ Å.

The larger value of $\Delta$ for 5′ entries accounts for the fact that 5′ activation times become progressively larger than 3′ ones as $F_s$ is lowered. The $\tau_a$ difference grows to several orders of magnitude when $F_s$ is extrapolated to 50−100 pN. Such forces are comparable to those exerted by the most powerful molecular motors,[31] and thus the very different activation times are consistent with the peculiar resistance of xrRNA to

degrading enzymes, which engage the 5′ end, while the same molecule can be processed from the 3′ end by replicases and reverse transcriptases.

*Translocation Duration.* We now focus on how translocation progresses once it initiates. Again, it is informative to contrast the observed behavior with that of standard homopolymers, where the typical time required to translocate a fraction $x$ of the chain scales asymptotically as $\tau_d \sim x^{1+\nu}F_s^{-1}$,[19,20,32−35] where $\nu$ is the metric exponent. The curves of Figure 2 depart qualitatively from this scaling law because the translocation does not proceed uniformly but presents systematic pauses and slowing downs in correspondence of precise xrRNA regions. We will discuss in more depth these properties further below where we connect them to the secondary and tertiary xrRNA organization. Here, we instead consider the overall duration of the translocation process, $\tau_d$, and its dependence on the applied force, $F_s$. The results are shown in Figure 3b, where two notable features are discernible.

First, the trend of $\tau_d$ vs $F_s^{-1}$ is visibly nonlinear for the 3′ end, the one with the widest range of $F_s^{-1}$. The nonlinearity marks a further difference from the homopolymer case, where the simpler dissipative process yields $\tau_d \propto F_s^{-1}$ (see above). Instead, the 3′ data are more compatible with two distinct linear regimes crossing over at $F_s \sim 130$ pN (inverse force of $0.76 \times 10^{-2}$ pN$^{-1}$).

Second, the $\tau_d$ data points are quite similar for the two ends. This is best appreciated in the inset of Figure 3b, which covers the region at small inverse forces (large $F_s$) for which data are available for both pulling directions. One notes that the 5′ data have only small deviations from the low-force linear branch of the 3′ entry case.

The microscopic origins of both features are discussed further below.

**Periodic Driving.** We next consider the xrRNA response to periodic driving. The setup is of interest for several reasons. First, it represents a still unexplored avenue where any novel insight can advance our understanding of RNA pore translocation. Second, it provides a term of reference for future electrokinetic experiments with, for example, solid state nanopores. Finally, the periodic driving mode is a simplified model for the action of enzymatic complexes that generally pull on the substrate in an intermittent and discontinuous manner.[36−39] These processive enzymes, which include exoribonucleases, are much larger than the xrRNA molecule
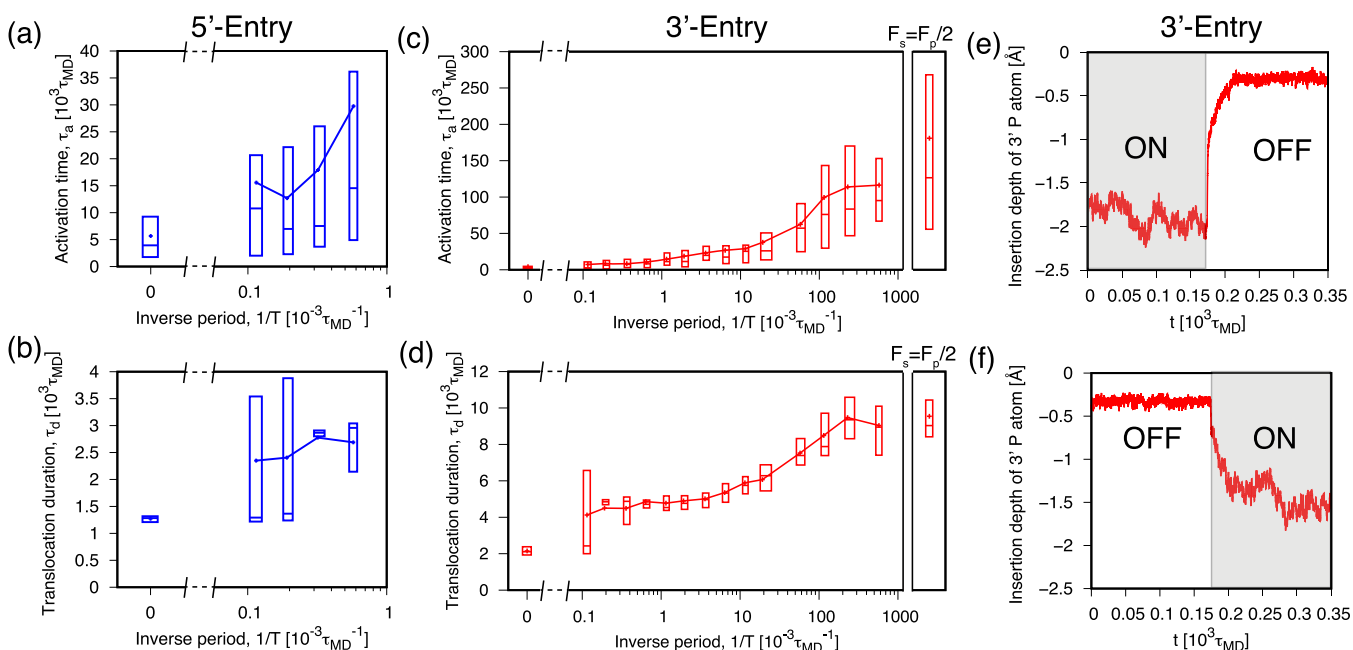
**Figure 5.** Translocation activation times and process duration for periodic driving forces. Box plots for (a) translocation activation times, $\tau_a$, and (b) translocation duration, $\tau_d$, for a periodically switched driving force, $F_p = 238$ pN, applied at the 5′ end. Corresponding plots for the 3′ end and $F_p = 177$ pN are given in panels c and d. The box plots at the right of these two panels show $\tau_a$ and $\tau_d$ for a static force equal to $F_s = F_p/2$; the data are a reference for the asymptotic case $1/T \rightarrow \infty$, i.e., $T \rightarrow 0$. The static case, instead, corresponds to $1/T = 0$. Panels e and f show the system response to the sudden switching on or off of a static force $F_s = 177$ pN applied to the 3′ end of the xrRNA. The response is monitored through the pore insertion depth of the 3′ P atom. The box plot drawing convention is the same as for Figure 3.

of interest, which makes it computationally impractical to use them in place of the cylindrical pore.

We adopted a square-wave driving mode, with the pulling force switched between $F_p$ ("on" phase) and 0 ("off" phase) at each semiperiod of duration $T/2$. For ease of comparison, we set $F_p$ equal to 238 and 177 pN at the 5′ and 3′ ends, respectively, as these forces yield about the same $\tau_a \sim (4-5) \times 10^3 \tau_{MD}$ at both ends in the static case. The period $T$ was varied in the $0.0017-8.7 \times 10^3 \tau_{MD}$ range, that is, from being much smaller than $\tau_a$ to being comparable to it. Longer switching times were not considered because a significant fraction of translocations would otherwise complete already in the first "on" cycle.

Typical translocation curves at $T = 5.2 \times 10^3 \tau_{MD}$ are shown in Figure 4. In this case, from two to three cycles are needed to activate the translocation process in half of the trajectories. The average activation times are equal to $12.7 \times 10^3 \tau_{MD}$ (5′ entry) and $8.6 \times 10^3 \tau_{MD}$ (3′ entry), which are larger than the corresponding static values by more than a factor of 2.

Only few translocations complete in the same cycle where they initiate, and these cases are more common for 5′ entries. Most trajectories require two cycles to complete translocation after initiation. During the "off" phase of these trajectories, the translocation process is not only paused but can even regress. Note that most of the pauses and chain retractions from the pore occur in the first part of the translocation process, regardless of the pulling direction. This aspect will be revisited and discussed more in detail in the next section.

A systematic overview of how the periodic driving affects $\tau_a$ and $\tau_d$ is given in Figure 5, where these quantities are plotted as a function of $1/T$. In the static limit, corresponding to $1/T = 0$, the activation times for 5′ and 3′ entries are about equal at the considered values of $F_p$. As $1/T$ is increased from zero, $\tau_a$ increases as well for both types of entries, though more

prominently for the 5′ one (see Figure 5a,c). A monotonic increase with $1/T$ is observed for the trajectory duration, too (see Figure 5b,d). In fact, $\tau_d$ approximately doubles going from the static case ($1/T = 0$) to $1/T \sim 0.6 \times 10^{-3} \tau_{MD}^{-1}$ for both ends.

The spread of the distributions of $\tau_d$ and $\tau_a$ increases with $1/T$, too. Both aspects reflects the occurrence of pauses and chain retractions during the intervening "off" phases which vary in number from one trajectory to the other and thus increase the duration and heterogeneity of the translocation process.

The limit $1/T \rightarrow \infty$ is noteworthy because, when the switching is much faster than the characteristic response time of the system, one expects to recover the same behavior as in the static case but with half the force, $F_s = F_p/2$. We discuss this limit for 3′ entries only, for which the activation and duration times remain computationally addressable as the switching interval is reduced. The results are shown in Figure 5c,d, where it is seen that, indeed, $\tau_a$ and $\tau_d$ become asymptotically compatible with the static values at half the force as $T \rightarrow 0$, i.e., $1/T \rightarrow \infty$. Notice that the crossover toward the asymptotic limit occurs for $T \sim 10\, \tau_{MD}$. This time duration is comparable to the system response time to a sudden switching of the pulling force $F_p$, which is about $50\, \tau_{MD}$ (see Figure 5e,f). The results thus indicate that the half-force static response can be observed only for switching intervals smaller than the characteristic response time of the system.

**Hindrance of Secondary and Tertiary Elements.** To locate specific xrRNA regions responsible for hindering translocation, we computed the so-called waiting time,[30] $w$, of each nucleotide. The observable, which is experimentally relevant in connection with ionic current blockade, measures how long a nucleotide takes, on average, to cross the *cis* region and enter the pore (see the Methods section).
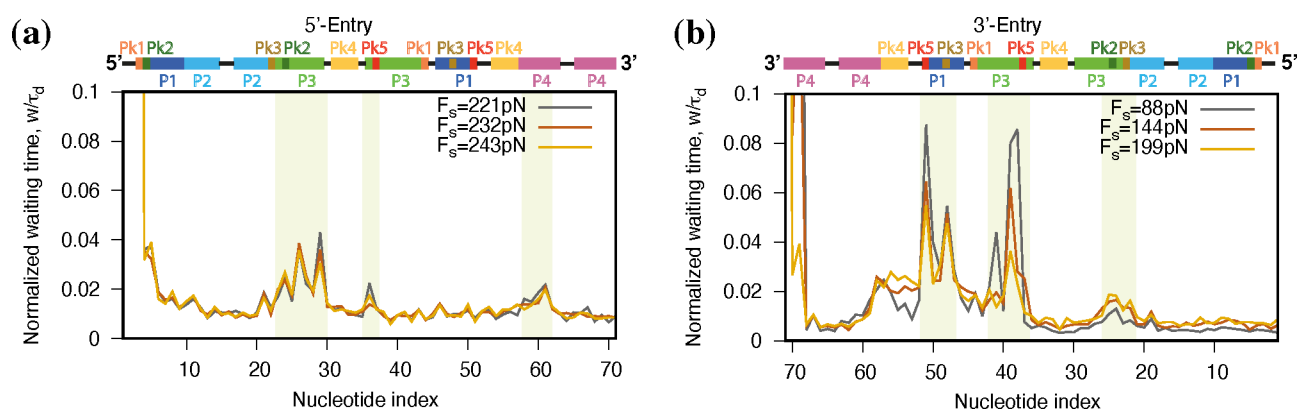
**Figure 6.** Site-dependent translocation hindrance; waiting times profiles. Waiting time profiles for three different static driving forces, $F_s$, applied to the (a) 5′ and (b) 3′ ends. The waiting time, $w$, of a nucleotide corresponds to the average time required to cross the *cis* region and enter the pore. For ease of comparison, the $w$ profiles are normalized to the average translocation duration. The off-scale values for nucleotides indexes smaller than 3 for the 5′ entry, and larger than 69 for the 3′ entry, reflect the typically large times required to activate translocation. The colored background highlights regions with the largest waiting times.

Typical waiting times profiles are shown in Figure 6. The data are for different static forces applied at the two xrRNA ends and are normalized by the average translocation duration, $\tau_d$, to facilitate comparison. The normalized $w$ profiles differ significantly from 5′ entries and 3′ entries, but within each of these two sets, they are consistent across the considered forces, which yield significant variations of $\tau_d$.

Qualitative differences for the two types of pore entries are not entirely unexpected, given earlier results on xrRNA directional resistance to translocation,[8] which, however, hinged on the analysis of activation times. Instead, the present results highlight differences in waiting times and thus provide a first insight into how diversely translocation proceeds from the two ends once it initiates.

We first discuss the $w$ profiles for 3′ entries (Figure 6b), which we could obtain for a wider range of forces thanks to the shorter translocation times. The largest resistance is offered by the stretch of nucleotides from U51 to A36 (ordered according to the 3′ → 5′ translocation direction), where two sets of peaks are observed. The first one involves Pk3 and Pk5, and the second involves the 3′ arms of helix P3. The height of these peaks is highest at low force. The remainder of the xrRNA structure beyond A36 offers relatively little hindrance, except for the neighborhood of Pk2.

The $w$ profiles for 5′ entries, which take much longer to translocate, were, by computational necessity, collected at higher forces (see Figure 6a). The first encountered and most prominent peak corresponds to the 5′ arm of helix P3, which includes the neighborhoods of Pk3. Two further minor peaks are observed close to the 5′ arm of Pk5 and helix P4.

The very different nature of the profiles at the two ends can be rationalized by considering the sequential order in which secondary elements are disrupted by translocation, and especially that helices can offer resistance only for the first translocating arm, after which they become fully unzipped.

These observations suffice to account for the qualitative features of the $w$ profiles for both types of pore entries. For 3′ entries, translocation initiates with the unzipping of the P4 helix. After this event, which is off-scale in Figure 6b, the first appreciable hindrance is encountered in correspondence of Pk3-Pk5. Translocation next proceeds with the disruption of the contacts in helix P3. Once the latter is unzipped, the remainder xrRNA structure is mostly void of secondary

elements, the residual ones being only Pk2 and P2 that translocate with little resistance. From a quantitative point of view, it is interesting that although the applied static force is constant throughout the translocation process, all helices P1 to P3 are disrupted in a small fraction of the time required to activate the unzipping of helix P4.

Analogous considerations apply to the 5′ end (Figure 6a). Here translocation initiates with the disruption of Pk1 and Pk2 (again, this event is off-scale in the graph of Figure 6a). No particular hindrance is found for P1 and P2, while more resistance is offered by the 5′ arm of P3. After P3 becomes unzipped, the only significant remaining secondary element is helix P4, and in fact, translocation proceeds unhindered up to this point, which defines the last obstacle of the process.

The single feature of the $w$ profiles that bears a noticeable force dependence is the height of the peaks in the 3′ arms of helices P1 and P3 of Figure 6b (3′ entry). The height of the peaks is strongly diminished when the applied force is increased. It is physically appealing to associate the decrease of normalized waiting times with a reduction of the free energy barriers hindering translocation. We accordingly surmise that the crossover between the two different linear regimes for $\tau_d$ in Figure 3b follows from a change of the unzipping barriers for P1 and P3. In support of this speculation we provide two observations. First, for $F_s \sim 144$ pN the peaks have an intermediate height between the maximum and minimum values, and this force is comparable to where the $\tau_d$ crossover is observed for $F_s \sim 130$ pN, see Figure 3b. Second, the milder slope of the high-force (small inverse forces) branch of $\tau_d$ is consistent with translocation barriers becoming smaller, as the peak waiting times, at large $F_s$.

## ■ SUMMARY AND CONCLUSIONS

Nanopore translocation is a powerful single-molecule probing technique that has been used in diverse contexts: from studying the physical response of homopolymers,[19−21,33,35,40] to the topological friction in chains with knots and links,[34,41−49] for sequencing and analyzing biopolymers' secondary and tertiary structures,[7,11,30,42,50−52,54−56,58] and study RNA, too.[1−4,6−8]

Here, we used nanopore translocation simulations to study the compliance of a viral RNA to be driven through a narrow pore. We focused on the 71-nucleotide-long xrRNA from the

Zika virus. In a previous atomistic study from our group,[8] the translocation response of the xrRNA was studied with a force-ramping protocol, a common setup for force spectroscopy experiments. The xrRNA was found to be capable of withstanding much higher pulling forces at the 5′ end than at the 3′ one before translocation could initiate. The strongly directional resistance was ascribed to the particular architecture of the xrRNA, which tightens, thus offering more resistance, when its 5′ region is pulled against the pore surface. The observed directional resistance is arguably harnessed by the molecule to elude the degrading action of cellular exonucleases, which engage RNAs from the 5′ end.[13−15]

Here, we used atomistic simulations and a native-centric model[25,26] to clarify three different aspects of RNA pore translocation: how the onset and duration of RNA translocation depend on the driving force, what are differences of using static or periodic driving modes, and how the progress of translocation is affected by secondary and tertiary elements.

We established the following results. First, the start of xrRNA translocation is so delayed with respect to the time of application of the driving forces that translocation activation times can exceed by orders of magnitude the duration of translocation process itself. In the static case, the force-dependent duration of the delays is compatible with a two-state activated process involving barriers of very different widths at the two ends. The barrier widths are not dissimilar from those estimated previously with the Bell−Evans analysis of force-ramped trajectories,[8] and the widest barrier ($5.6 \pm 0.2$ Å) is encountered at the 5′ end. This implies that the relative difference in activation times at the two ends grows exponentially as the pulling force is lowered.

Second, we observe that using a periodic driving instead of a static one increases significantly both the activation times and the duration of the process. The variance of both quantities is increased with respect to the static case, too. Both aspects are accounted for by the fact that the process is stalled and can even regress during the off phase of the driving cycle. We thus conclude that the directional resistance of xrRNA is enhanced by discontinuous pulling modes, such as those that arguably occur *in vivo* when the xrRNA is engaged by processive enzymes, such as exonucleases, replicases, and reverse-transcriptases.

Finally, we investigated the nonuniform progress of translocation once started. Regardless of the pulling directionality, the largest hindrance is always encountered in the first part of the trajectory. Analysis of the waiting times profiles provides a simple rationale for this result: secondary elements such as helices can offer resistance only for one of their two arms, the one pulled first into the pore, after which they become fully unzipped. Consequently, as translocation progresses, the RNA becomes rapidly depleted of intact secondary elements, and the process can proceed with less and less hindrance. More quantitatively, we pinpointed the specific xrRNA regions most responsible for hindering translocation. These regions are different for the two pulling ends, but in both cases, they involve helix P3 which includes pseudoknotted nucleotides.

The findings are of interest and have implications beyond the case of Zika xrRNA, as they highlight the several ways in which the translocation of folded RNAs differs from that of homopolymers. For general models of homopolymers, which are exclusively informed by chain connectivity and excluded volume interactions, translocation can initiate concomitantly with the application of the driving force and then proceeds smoothly following an asymptotic scaling law defined by the metric exponent.[33,35] We instead observe that folded RNAs, which are stabilized by specific intramolecular interactions, present major delays in the start of translocation. In fact, the activation times can exceed by far the duration of translocation itself. In addition, rather than proceeding smoothly, xrRNA translocations present slowing downs, pauses, and even retractions that, though depending on pulling directionality, occur in correspondence of specific secondary and tertiary elements.

The results complement and generalize previous studies of translocating RNA hairpins[53,59,60] and offer valuable terms of reference for future theoretical and experimental studies. In particular, the results ought to be useful to validate simpler RNA models, for example, based on coarser structural descriptions and effective intramolecular interactions, which would be more amenable to numerical characterization and hence more widely applicable. Natural targets of such endeavors would be other viral RNAs, especially those already known to be capable of resisting degradation by exonucleases.[14,61,62] In addition, we expect that the present elucidation of the interplay of translocation directionality, pulling mode, and RNAs' secondary and tertiary structures ought to be useful for interpreting and, possibly, designing future single-molecule experiments. For both theory and experiment, we believe that a promising avenue would be to extend considerations to how exactly processive enzymes engage and translocate RNAs with complex architectures.

## ■ AUTHOR INFORMATION

### Corresponding Author

**Cristian Micheletti** − *Physics Area, Scuola Internazionale Superiore di Studi Avanzati (SISSA), 34136 Trieste, Italy;* ⊙ orcid.org/0000-0002-1022-1638; Email: michelet@sissa.it

### Authors

**Matteo Becchi** − *Physics Area, Scuola Internazionale Superiore di Studi Avanzati (SISSA), 34136 Trieste, Italy;* ⊙ orcid.org/0000-0002-6306-5229

**Pietro Chiarantoni** − *Physics Area, Scuola Internazionale Superiore di Studi Avanzati (SISSA), 34136 Trieste, Italy;* ⊙ orcid.org/0000-0002-9249-863X

**Antonio Suma** − *Dipartimento di Fisica, Università di Bari and Sezione INFN di Bari, 70126 Bari, Italy;* ⊙ orcid.org/0000-0002-5049-9255

Complete contact information is available at:
https://pubs.acs.org/10.1021/acs.jpcb.0c09966

### Author Contributions

#M.B. and P.C. contributed equally.

### Notes

The authors declare no competing financial interest.

## ■ REFERENCES

(1) Smith, A. M.; Abu-Shumays, R.; Akeson, M.; Bernick, D. L. Capture, unfolding, and detection of individual tRNA molecules using a nanopore device. *Front. Bioeng. Biotechnol.* **2015**, *3*, 91.

(2) Rozevsky, Y.; Gilboa, T.; van Kooten, X. F.; Kobelt, D.; Huttner, D.; Stein, U.; Meller, A. Quantification of mRNA expression using single-molecule nanopore sensing. *ACS Nano* **2020**, *14*, 13964−13974.

(3) Butler, T. Z.; Gundlach, J. H.; Troll, M. Ionic current blockades from DNA and RNA molecules in the $\alpha$-hemolysin nanopore. *Biophys. J.* **2007**, *93*, 3229−3240.

(4) Garalde, D. R.; Snell, E. A.; Jachimowicz, D.; Sipos, B.; Lloyd, J. H.; Bruce, M.; Pantic, N.; Admassu, T.; James, P.; Warland, A.; et al. Highly parallel direct RNA sequencing on an array of nanopores. *Nat. Methods* **2018**, *15*, 201.

(5) Zhang, X.; Zhang, D.; Zhao, C.; Tian, K.; Shi, R.; Du, X.; Burcke, A. J.; Wang, J.; Chen, S.-J.; Gu, L.-Q. Nanopore electric snapshots of an RNA tertiary folding pathway. *Nat. Commun.* **2017**, *8*, 1−11.

(6) Smith, A. M.; Jain, M.; Mulroney, L.; Garalde, D. R.; Akeson, M. Reading canonical and modified nucleobases in 16S ribosomal RNA using nanopore native RNA sequencing. *PLoS One* **2019**, *14*, e0216709.

(7) Bandarkar, P.; Yang, H.; Henley, R. Y.; Wanunu, M.; Whitford, P. C. How nanopore translocation experiments can measure RNA unfolding. *Biophys. J.* **2020**, *118*, 1612.

(8) Suma, A.; Coronel, L.; Bussi, G.; Micheletti, C. Directional translocation resistance of Zika xrRNA. *Nat. Commun.* **2020**, *11*, 1−9.

(9) Giedroc, D. P.; Cornish, P. V. Frameshifting RNA pseudoknots: structure and mechanism. *Virus Res.* **2009**, *139*, 193−208.

(10) Giedroc, D. P.; Theimer, C. A.; Nixon, P. L. Structure, stability and function of RNA pseudoknots involved in stimulating ribosomal frameshifting. *J. Mol. Biol.* **2000**, *298*, 167−185.

(11) Chen, G.; Chang, K.-Y.; Chou, M.-Y.; Bustamante, C.; Tinoco, I. Triplex structures in an RNA pseudoknot enhance mechanical stability and increase efficiency of-1 ribosomal frameshifting. *Proc. Natl. Acad. Sci. U. S. A.* **2009**, *106*, 12706−12711.

(12) Le, S.-Y.; Shapiro, B. A.; Chen, J.-H.; Nussinov, R.; Maizel, J. V. RNA pseudoknots downstream of the frameshift sites of retroviruses. *Genet. Anal.: Tech. Appl.* **1991**, *8*, 191−205.

(13) Pijlman, G. P.; Funk, A.; Kondratieva, N.; Leung, J.; Torres, S.; Van der Aa, L.; Liu, W. J.; Palmenberg, A. C.; Shi, P.-Y.; Hall, R. A.; Khromykh, A. A. A highly structured, nuclease-resistant, noncoding RNA produced by flaviviruses is required for pathogenicity. *Cell Host Microbe* **2008**, *4*, 579−591.

(14) Chapman, E. G.; Costantino, D. A.; Rabe, J. L.; Moon, S. L.; Wilusz, J.; Nix, J. C.; Kieft, J. S. The structural basis of pathogenic subgenomic flavivirus RNA (sfRNA) production. *Science* **2014**, *344*, 307−310.

(15) Akiyama, B. M.; Laurence, H. M.; Massey, A. R.; Costantino, D. A.; Xie, X.; Yang, Y.; Shi, P.-Y.; Nix, J. C.; Beckham, J. D.; Kieft, J. S. Zika virus produces noncoding RNAs using a multi-pseudoknot structure that confounds a cellular exonuclease. *Science* **2016**, *354*, 1148−1152.

(16) Slonchak, A.; Khromykh, A. A. Subgenomic flaviviral RNAs: What do we know after the first decade of research. *Antiviral Res.* **2018**, *159*, 13.

(17) MacFadden, A.; O'Donoghue, Z.; Silva, P. A.; Chapman, E. G.; Olsthoorn, R. C.; Sterken, M. G.; Pijlman, G. P.; Bredenbeek, P. J.; Kieft, J. S. Mechanism and structural diversity of exoribonuclease-resistant RNA structures in flaviviral RNAs. *Nat. Commun.* **2018**, *9*, 119.

(18) Ng, W. C.; Soto-Acosta, R.; Bradrick, S. S.; Garcia-Blanco, M. A.; Ooi, E. E. The 5′ and 3′ untranslated regions of the flaviviral genome. *Viruses* **2017**, *9*, 137.

(19) Kantor, Y.; Kardar, M. Anomalous dynamics of forced translocation. *Phys. Rev. E* **2004**, *69*, 021806.

(20) Rowghanian, P.; Grosberg, A. Y. Propagation of tension along a polymer chain. *Phys. Rev. E* **2012**, *86*, 011803.

(21) Palyulin, V. V.; Ala-Nissila, T.; Metzler, R. Polymer translocation: the first two decades and the recent diversification. *Soft Matter* **2014**, *10*, 9016−9037.

(22) Humphrey, W.; Dalke, A.; Schulten, K. Visual Molecular Dynamics. *J. Mol. Graphics* **1996**, *14*, 33−38.

(23) Berman, H. M.; Bourne, P. E.; Westbrook, J.; Zardecki, C. *Protein Structure*; CRC Press: 2003; pp 394−410.

(24) Jinek, M.; Coyle, S. M.; Doudna, J. A. Coupled 5′ nucleotide recognition and processivity in Xrn1-mediated mRNA decay. *Mol. Cell* **2011**, *41*, 600−608.

(25) Whitford, P. C.; Noel, J. K.; Gosavi, S.; Schug, A.; Sanbonmatsu, K. Y.; Onuchic, J. N. An all-atom structure-based potential for proteins: bridging minimal models with all-atom empirical forcefields. *Proteins: Struct., Funct., Genet.* **2009**, *75*, 430−441.

(26) Noel, J. K.; Levi, M.; Raghunathan, M.; Lammert, H.; Hayes, R. L.; Onuchic, J. N.; Whitford, P. C. SMOG 2: A versatile software package for generating structure-based models. *PLoS Comput. Biol.* **2016**, *12*, e1004794.

(27) Plimpton, S. Fast parallel algorithms for short-range molecular dynamics. *J. Comput. Phys.* **1995**, *117*, 1−19.

(28) SMOG to LAMMPS Converter; github.com/CristianMicheletti/SMOG-converter.

(29) Yang, H.; Bandarkar, P.; Horne, R.; Leite, V. B.; Chahine, J.; Whitford, P. C. Diffusion of tRNA inside the ribosome is position-dependent. *J. Chem. Phys.* **2019**, *151*, 085102.

(30) Luo, K.; Ala-Nissila, T.; Ying, S.-C.; Bhattacharya, A. Sequence dependence of DNA translocation through a nanopore. *Phys. Rev. Lett.* **2008**, *100*, 058101.

(31) Smith, D. E.; Tans, S. J.; Smith, S. B.; Grimes, S.; Anderson, D. L.; Bustamante, C. The bacteriophage $\varphi$29 portal motor can package DNA against a large internal force. *Nature* **2001**, *413*, 748−752.

(32) Sakaue, T. Nonequilibrium dynamics of polymer translocation and straightening. *Phys. Rev. E* **2007**, *76*, 021803.

(33) Ikonen, T.; Bhattacharya, A.; Ala-Nissila, T.; Sung, W. Unifying model of driven polymer translocation. *Phys. Rev. E* **2012**, *85*, 051803.

(34) Rosa, A.; Di Ventra, M.; Micheletti, C. Topological jamming of spontaneously knotted polyelectrolyte chains driven through a nanopore. *Phys. Rev. Lett.* **2012**, *109*, 118301.

(35) Sarabadani, J.; Ala-Nissila, T. Theory of pore-driven and end-pulled polymer translocation dynamics through a nanopore: An overview. *J. Phys.: Condens. Matter* **2018**, *30*, 274002.

(36) Kravats, A.; Jayasinghe, M.; Stan, G. Unfolding and trans-location pathway of substrate protein controlled by structure in repetitive allosteric cycles of the ClpY ATPase. *Proc. Natl. Acad. Sci. U. S. A.* **2011**, *108*, 2234−2239.

(37) Wojciechowski, M.; Szymczak, P.; Carrión-Vázquez, M.; Cieplak, M. Protein unfolding by biological unfoldases: Insights from modeling. *Biophys. J.* **2014**, *107*, 1661−1668.

(38) Sarabadani, J.; Ikonen, T.; Ala-Nissila, T. Theory of polymer translocation through a flickering nanopore under an alternating driving force. *J. Chem. Phys.* **2015**, *143*, 074905.

(39) Szymczak, P. Periodic forces trigger knot untying during translocation of knotted proteins. *Sci. Rep.* **2016**, *6*, 1−10.

(40) Muthukumar, M. Mechanism of DNA transport through pores. *Annu. Rev. Biophys. Biomol. Struct.* **2007**, *36*, 435−450.

(41) Suma, A.; Rosa, A.; Micheletti, C. Pore translocation of knotted polymer chains: How friction depends on knot complexity. *ACS Macro Lett.* **2015**, *4*, 1420−1424.

(42) Plesa, C.; Verschueren, D.; Pud, S.; van der Torre, J.; Ruitenberg, J. W.; Witteveen, M. J.; Jonsson, M. P.; Grosberg, A. Y.; Rabin, Y.; Dekker, C. Direct observation of DNA knots using a solid-state nanopore. *Nat. Nanotechnol.* **2016**, *11*, 1093.

(43) San Martín, Á.; Rodriguez-Aliaga, P.; Molina, J. A.; Martin, A.; Bustamante, C.; Baez, M. Knots can impair protein degradation by ATP-dependent proteases. *Proc. Natl. Acad. Sci. U. S. A.* **2017**, *114*, 9864−9869.

(44) Suma, A.; Micheletti, C. Pore translocation of knotted DNA rings. *Proc. Natl. Acad. Sci. U. S. A.* **2017**, *114*, E2991−E2997.

(45) Sriramoju, M. K.; Chen, Y.; Lee, Y.-T. C.; Hsu, S.-T. D. Topologically knotted deubiquitinases exhibit unprecedented mechanostability to withstand the proteolysis by an AAA+ protease. *Sci. Rep.* **2018**, *8*, 7076.

(46) Sivertsson, E. M.; Jackson, S. E.; Itzhaki, L. S. The AAA+ protease ClpXP can easily degrade a 3 1 and a 5 2-knotted protein. *Sci. Rep.* **2019**, *9*, 1−14.

(47) Sharma, R. K.; Agrawal, I.; Dai, L.; Doyle, P. S.; Garaj, S. Complex DNA knots detected with a nanopore sensor. *Nat. Commun.* **2019**, *10*, 1−9.

(48) Caraglio, M.; Orlandini, E.; Whittington, S. Driven Translocation of Linked Ring Polymers through a Pore. *Macromolecules* **2017**, *50*, 9437−9444.

(49) Caraglio, M.; Orlandini, E.; Whittington, S. G. Translocation of links through a pore: effects of link complexity and size. *J. Stat. Mech.: Theory Exp.* **2020**, *2020*, 043203.

(50) Meller, A.; Nivon, L.; Branton, D. Voltage-driven DNA translocations through a nanopore. *Phys. Rev. Lett.* **2001**, *86*, 3435.

(51) Trepagnier, E. H.; Radenovic, A.; Sivak, D.; Geissler, P.; Liphardt, J. Controlling DNA capture and propagation through artificial nanopores. *Nano Lett.* **2007**, *7*, 2824−2830.

(52) Comer, J.; Dimitrov, V.; Zhao, Q.; Timp, G.; Aksimentiev, A. Microscopic mechanics of hairpin DNA translocation through synthetic nanopores. *Biophys. J.* **2009**, *96*, 593−608.

(53) Henley, R. Y.; Carson, S.; Wanunu, M. *Prog. Mol. Biol. Transl.* **2016**, *139*, 73−99.

(54) Zwolak, M.; Di Ventra, M. Colloquium: Physical approaches to DNA sequencing and detection. *Rev. Mod. Phys.* **2008**, *80*, 141.

(55) Branton, D.; Deamer, D. W.; Marziali, A.; Bayley, H.; Benner, S. A.; Butler, T.; Di Ventra, M.; Garaj, S.; Hibbs, A.; Huang, X.; et al. The potential and challenges of nanopore sequencing. *Nat. Biotechnol.* **2008**, *26*, 1146−1153.

(56) Cao, C.; Li, M.-Y.; Cirauqui, N.; Wang, Y.-Q.; Dal Peraro, M.; Tian, H.; Long, Y.-T. Mapping the sensing spots of aerolysin for single oligonucleotides analysis. *Nat. Commun.* **2018**, *9*, 1−9.

(57) Merchant, C. A.; Healy, K.; Wanunu, M.; Ray, V.; Peterman, N.; Bartel, J.; Fischbein, M. D.; Venta, K.; Luo, Z.; Johnson, A. C.; et al. DNA translocation through graphene nanopores. *Nano Lett.* **2010**, *10*, 2915−2921.

(58) Kubota, T.; Lloyd, K.; Sakashita, N.; Minato, S.; Ishida, K.; Mitsui, T. Clog and Release, and Reverse Motions of DNA in a Nanopore. *Polymers* **2019**, *11*, 84.

(59) Wen, J.-D.; Manosas, M.; Li, P. T.; Smith, S. B.; Bustamante, C.; Ritort, F.; Tinoco, I., Jr. Force unfolding kinetics of RNA using optical tweezers. *Biophys. J.* **2007**, *92*, 2996−3009.

(60) Manosas, M.; Collin, D.; Ritort, F. Force-dependent fragility in RNA hairpins. *Phys. Rev. Lett.* **2006**, *96*, 218301.

(61) Steckelberg, A.-L.; Akiyama, B. M.; Costantino, D. A.; Sit, T. L.; Nix, J. C.; Kieft, J. S. A folded viral noncoding RNA blocks host cell exoribonucleases through a conformationally dynamic RNA structure. *Proc. Natl. Acad. Sci. U. S. A.* **2018**, *115*, 6404−6409.

(62) Jones, R. A.; Steckelberg, A.-L.; Vicens, Q.; Szucs, M. J.; Akiyama, B. M.; Kieft, J. S. Different tertiary interactions create the same important 3D features in a distinct flavivirus xrRNA. *RNA* **2021**, *27*, 54−65.